Journal of Materials Chemistry A

COMMUNICATION

View Article Online
View Journal | View Issue

Cite this: J. Mater. Chem. A, 2015, 3, 21434

Received 3rd September 2015
Accepted 3rd October 2015

DOI: 10.1039/c5ta07003a

www.rsc.org/MaterialsA

Facile synthesis of an iron doped rutile TiO_2 photocatalyst for enhanced visible-light-driven water oxidation†

Junqing Yan,[ac] Yunxia Zhang,[c] Shengzhong Liu,*[c] Guangjun Wu,[ab] Landong Li*[ab] and Naijia Guan[ab]

A facile fast hydrolysis route to a three-dimensional flow-like iron doped rutile TiO_2 nanostructure is developed. With iron species doping into both the bulk phase and the surface, the bandgap narrowing of rutile TiO_2 is realized and the dissociative adsorption of water on the surface is promoted, which accordingly lead to greatly enhanced activity in visible-light-driven water oxidation.

Heterogeneous semiconductor photocatalysis has been developed as a promising approach to solve the energy crisis through the chemical utilization of renewable solar energy resources, since the discovery of water photolysis on a TiO_2 photoanode in 1972.[1–3] Among various semiconductor materials investigated, TiO_2 is considered as a benchmark photocatalyst owing to its satisfactory photocatalytic activity and good chemical stability.[4–6] However, TiO_2 possesses a wide bandgap of 3.0–3.2 eV and it can be only activated using ultraviolet light with wavelengths up to 400 nm, which occupies only 4% of the whole solar spectrum. To expand the working spectrum of TiO_2 to the visible light region for potential solar-light-driven photocatalysis, a general and effective strategy is disrupting the integrity of the lattice structure of pristine TiO_2, *e.g.* through element doping,[7–9] Ti^{3+} self-doping[10] and hydrogenation.[11]

The splitting of water into hydrogen and oxygen using a photocatalyst is a dream process for the direct absorption and conservation of solar energy.[3] To date, impressive photocatalytic efficiencies have been achieved in the reduction of water to hydrogen, *i.e.* half-reaction of water splitting, with TiO_2-based semiconductors.[11,12] It is generally acknowledged that the process of two-electron proton reduction is relatively easy to realize, while the oxidation of water to oxygen, the other half-reaction of water splitting involving short-life photo-generated holes in the four-electron process, is rather slow.[13–15] Meanwhile, it is also known that the valence band edge of TiO_2 is much more positive than the potential of water oxidation and, theoretically, TiO_2 should be a good candidate for water oxidation. Recently, some achievements have been made in water oxidation with TiO_2-based photocatalysts;[7,13] however, there is still much room for the water photo-oxidation efficiency, especially under visible-light irradiation. For the photocatalytic water oxidation on the TiO_2 surface, the molecular water or hydroxyl groups on the surface titanium sites are difficult to oxidize by photo-generated holes due to the reduced electron density of oxygen atoms by their electron donation to titanium atoms. Thus, surface modifications of TiO_2 should be necessary and also effective for promoting water oxidation through changing water adsorption behaviours. Typically, surface fluorination is tactfully developed for the alternation of the water adsorption mode on TiO_2, which facilitates hole transfer to the water molecules and the cleavage of O–H bonds by a proton-coupled electron transfer process.[16]

In our previous study, sub-10 nm rutile TiO_2 nanoparticles with a narrow bandgap of 2.7 eV were successfully prepared *via* a fast hydrolysis route and they exhibited very high activity in the visible-light-driven reduction of water to hydrogen.[12] These rutile TiO_2 nanoparticles also exhibited distinct activity in the photocatalytic oxidation of water to oxygen; however, the activity is not satisfactory (Fig. S1†) and the oxygen vacancies in rutile TiO_2 might be healed during water oxidation. On the basis of literature reports and our previous work, we design here iron doped rutile TiO_2 nanoparticles for possible photocatalytic oxygen evolution from water splitting. It is expected that the iron atoms in the bulk phase of rutile can extend the working spectrum of TiO_2 to the visible light region, while the surface iron atoms can change the adsorption of water through replacing tetravalent titanium atoms by trivalent iron atoms.

[a]School of Material Science and Engineering & National Institute for Advanced Materials, Nankai University, Tianjin, 30071, P. R. China

[b]Key Laboratory of Advanced Energy Materials Chemistry (Ministry of Education), Collaborative Innovation Center of Chemical Science and Engineering, Tianjin, 30071, P. R. China. E-mail: lild@nankai.edu.cn; Tel: +86-22-2350-0341

[c]Key Laboratory of Applied Surface and Colloid Chemistry (Ministry of Education), Institute for Advanced Energy Materials, School of Materials Science and Engineering, Shaanxi Normal University, Xi'an, 710119, P. R. China. E-mail: szliu@dicp.ac.cn

† Electronic supplementary information (ESI) available: Experimental details and characterization results. See DOI: 10.1039/c5ta07003a

Rutile TiO_2 and iron doped rutile TiO_2 were prepared *via* fast hydrolysis, followed by annealing in air at 773 K for 4 h (see ESI† for experimental details). Ferric trichloride was chosen as the iron precursor and a low Fe weight fraction of 0.1–1% was employed in this study. XRD patterns (Fig. S2†) reveal that all the samples obtained are of pure rutile phase (JCPDF# 21-1276),[17] and no iron oxide phase can be observed due to the low iron loading. On the other hand, a slight shift of the (110) peak of studied samples toward a higher angle could be observed after iron doping (Fig. S2†). The ionic radius of iron is smaller than that of titanium,[17] and the corresponding interplanar spacing distance of TiO_2 (110) will be reduced with the replacement of titanium atoms by iron atoms, as reflected by the shift of the (110) diffraction peak.

Raman spectroscopy was used to further investigate the crystalline structure and the results are given in Fig. 1a. Three major Raman-active modes of rutile TiO_2, *i.e.* a multi-proton process at 230 cm^{-1}, E_g at 445 cm^{-1} and A_{1g} at 610 cm^{-1},[18,19] are clearly observed for rutile TiO_2 and iron doped samples. Since the E_g mode is caused by the symmetric stretching vibration of O–Ti–O in TiO_2, doping TiO_2 with iron will result in a slight decrease in the relative intensity of E_g to A_{1g}, as revealed in Fig. 1a. Generally, replacing two adjacent titanium atoms by iron atoms will generate one oxygen vacancy and, therefore, weaken the symmetric stretching vibration of O–Ti–O. To examine the surface and sub-surface states of TiO_2 and Fe–TiO_2 samples, XPS analysis was employed and the results are shown in Fig. 1b. From Ti 2p core-level spectra, typical binding energy values at 458.3 and 464.1 eV, corresponding to $2p_{3/2}$ and $2p_{1/2}$ of Ti^{4+} in TiO_2, are clearly observed for all samples. No obvious Ti^{3+} signal can be detected, indicating the identical existence state of titanium atoms in TiO_2 and Fe–TiO_2 samples. In the Fe 2p XP spectra, a binding energy value of 711.1 eV, corresponding to the Fe^{3+} signal,[20] can be observed for Fe–TiO_2 samples at relatively high iron loadings of 0.3 and 0.5% (Fig. S3†). In the O 1s XP spectra, binding energy values of 529.7, 531.8 and 533.4 eV can be observed for all samples. The binding energy value of 529.7 eV is due to crystal lattice oxygen in O–Ti^{4+} (O_L). The binding energy values of 531.8 and 533.4 eV are due to the hydroxyl groups, *i.e.* Ti–OH and H_2O, respectively, strongly bound to the surface.[18,21] Interestingly, rutile TiO_2 shows the highest relative intensity of the hydroxyl groups and the intensity decreases distinctly with the iron doping level (Fig. 1b). It is known that the oxygen vacancies in rutile TiO_2 are always unstable and one oxygen vacancy can be oxidized by water to generate two hydroxyl groups.[22] These hydroxyl groups show great advantages in some photocatalytic applications of rutile TiO_2, *e.g.* water reduction;[12] however, they are not good for the water oxidation process.[16] In contrast to Fe–TiO_2, the oxygen vacancies neighbouring Fe^{3+} sites are very stable and they can act as electron scavengers for absorption of the hydrogen in water to form hydrogen bonds (Fig. S4†). On the basis of the above-mentioned characterization results, the structure model iron doped TiO_2 sample is illustrated in Fig. 1c.

The morphology of iron doped rutile TiO_2 samples was investigated by electron microscopy technology. As shown in the SEM images in Fig. S5,† all Fe doped samples present a similar three-dimensional flower-like structure, which is believed to be good for the light absorption and can promote the photocatalytic process.[23,24] Fig. 2a shows the typical TEM image of the 0.3% Fe–TiO_2 sample and a uniform flower-like structure can be clearly observed. The electron diffraction pattern of one petal of the flower (Fig. 2b) reveals the typical polycrystalline structure of rutile TiO_2. The high-resolution TEM image in Fig. 2c shows the lattice structure of rutile TiO_2, indicating its high degree of crystallinity and the HRTEM-based FFT analysis confirms the tetragonal structure (Fig. 2c inset). It should be mentioned that the interplanar spacing of 0.33 nm was observed for the TiO_2 and iron doped TiO_2 samples (Fig. S6†), corresponding to the most stable {110} facets in rutile.[25] The slight decrease in the interplanar spacing distance caused by the replacement of titanium atoms by iron atoms, as

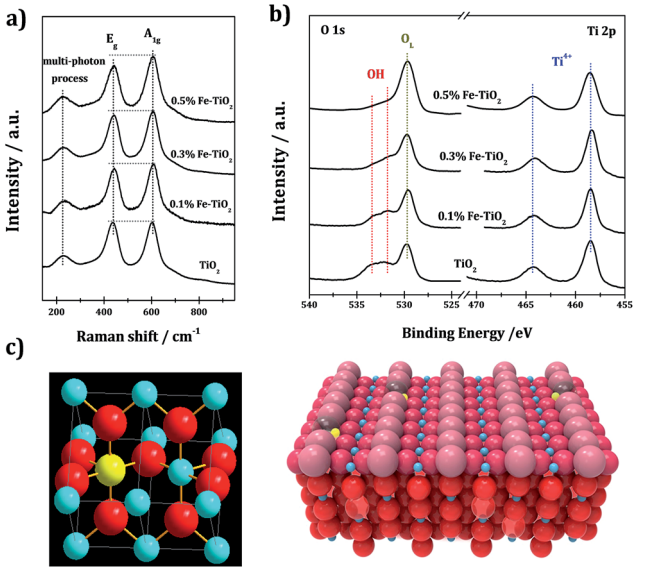

Fig. 1 (a) Raman spectra of rutile TiO_2 and iron doped TiO_2 samples; (b) O 1s and Ti 2p XPS of rutile TiO_2 and iron doped TiO_2 samples; (c) structure model of the iron doped TiO_2 sample.

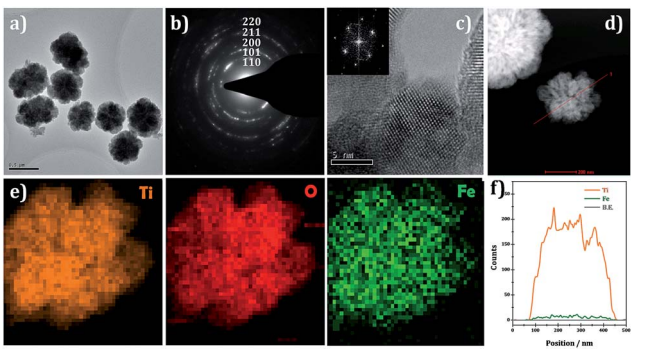

Fig. 2 (a) TEM image of the 0.3% Fe–TiO_2 sample; (b) electron diffraction pattern of the "+" region in (a); (c) HRTEM of the 0.3% Fe–TiO_2 sample and the corresponding FFT analysis result; (d) dark field TEM image of the 0.3% Fe–TiO_2 sample; (e and f) elemental area & line mapping results of the selected region in (d).

reflected in XRD patterns (Fig. S2†), is not observed in TEM images. However, a distinct increase in the surface roughness could be observed with iron doping into rutile TiO_2 (Fig. S6†). To obtain the direct evidence on iron element distribution in rutile TiO_2, we performed the elemental area & line mapping analysis and the results are shown in Fig. 2e and f, respectively. Elemental area mapping results clearly reveal the uniform distribution of iron atoms in rutile TiO_2 flower-like aggregates. The line mapping results agree well with the area mapping results and further indicate that the doped iron atoms are located both in the bulk phase and on the surface of the rutile TiO_2.

The optical properties of rutile TiO_2 and iron doped rutile TiO_2 samples are analysed by diffuse reflectance UV-vis spectroscopy and the results are shown in Fig. 3a. It is seen that iron doped rutile TiO_2 samples exhibit significant visible light absorption up to 700 nm and the visible light absorption increases with increasing iron loading from 0.1 to 0.5%. The bandgap of 0.3% Fe–TiO_2 is determined to be *ca.* 2.5 eV according to the plots of transformed Kubelka–Munk function *versus* the energy of light (Fig. 3b), *ca.* 0.4 eV lower than that of rutile TiO_2. The bandgap narrowing of rutile TiO_2 induced by iron doping is thus clearly illustrated. For a better understanding of the bandgap state of the iron doped rutile TiO_2 sample, VB-XPS and Mott–Schottky analyses were performed on 0.3% Fe–TiO_2. As shown in Fig. 3c, the valence band potential of 0.3% Fe–TiO_2 is estimated to be 0.3 eV more negative than that of undoped rutile TiO_2. That is, a *ca.* 0.3 eV upward shift in the valence band of rutile TiO_2 is obtained upon iron doping. In the Schottky plots in Fig. 3d, both rutile TiO_2 and 0.3% Fe–TiO_2 show positive slopes, confirming that iron doping into the rutile TiO_2 lattice will not change its n-type semiconductor properties. The flat-band potential of 0.3% Fe–TiO_2, obtained by the extrapolation of the Mott–Schottky plots, is 0.2 eV more positive than that of undoped rutile TiO_2. Since the conduction band potentials of n-type semiconductors are very close to the flat-band potentials,[26] it can be deduced that the conduction band of 0.3% Fe–TiO_2 is *ca.* 0.2 eV more positive than undoped rutile TiO_2. That is, a *ca.* 0.2 eV downward shift in the valence band of rutile TiO_2 is also obtained upon iron doping. On the basis of VB-XPS and Mott–Schottky plots, it is very clear that iron doping into rutile TiO_2 can simultaneously induce an upward shift in the valance band and a downward shift in the conduction band, resulting in the bandgap narrowing of rutile TiO_2 (Fig. 3b). The bandgap narrowing of rutile TiO_2 upon iron doping can be explained by the formation of sub-bands originating from the Ti–O–Fe interfacial bond and introduction of oxygen vacancies.[27,28] According to the specific bandgap construction, 0.3% Fe–TiO_2 is not a good photocatalyst for hydrogen generation since its conduction band might be lower than the redox potential of H_2/H_2O (in fact, no hydrogen production can be detected in the water splitting over 0.3% Fe–TiO_2 with methanol as the sacrificial reagent under UV-vis light), while 0.3% Fe–TiO_2 should be a good choice for the semiconductor photocatalyst for water oxidation to oxygen, even under the irradiation of visible light.

The photocatalytic oxygen evolution from water splitting was evaluated under irradiation of UV-vis light at 320–780 nm or visible light at 400–780 nm. It is clearly seen that iron doped rutile TiO_2 samples exhibit a greatly enhanced oxygen evolution rate as compared to un-doped reference rutile TiO_2 under both UV-vis and visible light irradiation (Fig. 4a). It is also seen that the promotion effects of iron doping are dependent on iron loading. The photocatalytic activity of rutile TiO_2 in oxygen evolution first increases with increasing iron loading, reaches a maximum at the loading of 0.3%, and then begins to decrease. Experimentally, 0.3% Fe–TiO_2 is optimized for further study, and the oxygen evolution rates of 24.6 μmol h^{-1} (246 μmol h^{-1}

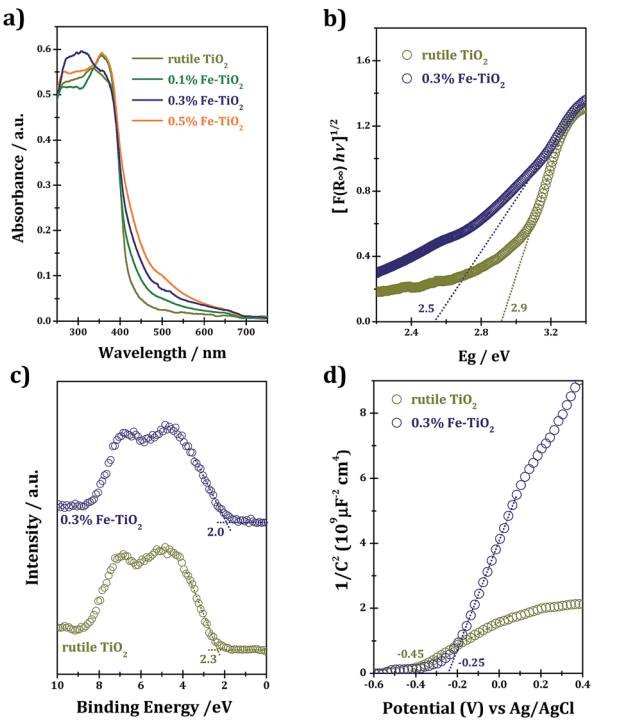

Fig. 3 (a and b) UV-vis spectra of rutile TiO_2 and iron doped rutile TiO_2 samples; (c) VB-XPS of rutile TiO_2 and 0.3% Fe–TiO_2; (d) Mott–Schottky plots of rutile TiO_2 and 0.3% Fe–TiO_2.

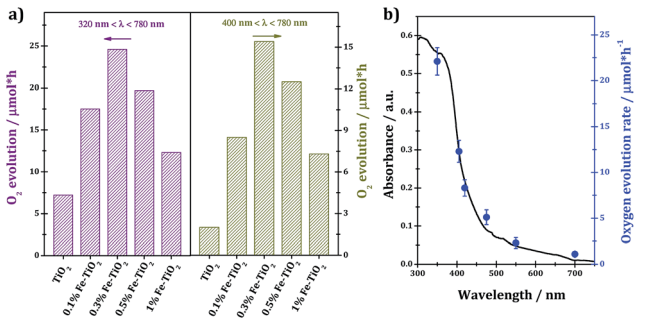

Fig. 4 (a) Photocatalytic oxygen evolution from water splitting over rutile TiO_2 and iron doped TiO_2 samples under the irradiation of UV-vis or visible light. Reaction conditions: 0.1 g photocatalyst, 100 mL 0.01 M $AgNO_3$ aqueous solution; (b) dependence of the oxygen evolution rate using 0.3% Fe–TiO_2 as a photocatalyst on the cutoff wavelength of incident light, along with the optical absorption spectrum.

g_{cat}^{-1}) and 15.4 μmol h^{-1} (154 μmol h^{-1} g_{cat}^{-1}) are obtained under UV-vis and visible light, respectively. To the best of our knowledge, these oxygen evolution rates are the highest ever reported for TiO_2-based materials under comparable conditions (also see apparent quantum yield reported in the following section).[29,30] It is known that defect sites will be introduced in pristine TiO_2 by element doping. A suitable amount of defect sites are good for the separation of photo-generated electrons–holes by trapping effects while excess defects will become the new recombination centres for photo-generated electrons–holes. Therefore, a certain amount of defects from element doping is required for the optimized semiconductor photocatalyst, and iron loading of 0.3% is optimized. This is confirmed by the room temperature photoluminescence spectroscopy analysis (Fig. S7†), where the lowest photoluminescence intensity is observed with 0.3% Fe–TiO_2. Another important issue to note is that the promotion effects of iron doping into rutile TiO_2 are much more significant under visible light (from 7.2 to 24.6 μmol h^{-1}) than those under UV-vis light (from 2.0 to 15.4 μmol h^{-1}). This should be due to the enhanced visible light absorption of rutile TiO_2 induced by iron doping in the bulk phase, as previously revealed by the UV-vis spectra (Fig. 3a). To disclose the role of surface iron species, experiments of TiO_2 surface modification (wet impregnation with $FeCl_3$ aqueous solution followed by calcination in the air) by using iron was further performed. As shown in Fig. S8,† TiO_2 surface modification with iron species can promote its photocatalytic activity in oxygen evolution to some extent, similarly to a previous report.[27] A higher amount of surface iron species (in the range of 0.02–0.06%) appears to be good for oxygen evolution. It is proposed that surface modification with iron can result in the formation of hydrogen bonds upon water adsorption (Fig. S4†), which facilitates the adsorption and dissociation of water. On the basis of the above-mentioned experimental results, the roles of iron doping in the visible-light-driven oxygen evolution over rutile TiO_2 can be concluded. On the one hand, the bulk Fe^{3+} sites in the lattice of the rutile structure can promote the visible light response of TiO_2 through replacing Ti^{4+} sites and creating oxygen vacancies. On the other hand, the surface Fe^{3+} sites can induce the formation of hydrogen bonds upon water adsorption and therefore facilitate water oxidation to dioxygen. It is demonstrated that iron doped rutile TiO_2 samples exhibit significant absorption in both ultraviolet and visible light regions. To explore the possible photocatalytic applications of iron doped rutile TiO_2 samples under real solar light, we further examined the dependence of activity on the wavelength of incident light. As shown in Fig. 4b, the photocatalytic activity of 0.3% Fe–TiO_2, expressed as the oxygen evolution rate, decreases with increasing incident light wavelength, matching perfectly with its optical absorption. Typically, the apparent quantum yields for oxygen evolution are calculated to be *ca.* 2.5, 1.8 and 0.8% at 405, 420 and 475 nm, respectively. These results clearly reveal that the photocatalytic oxygen evolution reaction occurs *via* light absorption by 0.3% Fe–TiO_2, which should be a robust photocatalyst for the reaction driven by solar light. On the basis of its physicochemical properties, Fe–TiO_2 should be a type of very stable photocatalyst, similar to reference rutile TiO_2. To verify this, the stability of 0.3% Fe–TiO_2 was tested in visible-light-driven RhB degradation (see ESI for details†) and the results are shown in Fig. S9.† It is seen that no activity loss could be observed within 3 cycles, demonstrating the good stability and recyclability of the iron doped rutile TiO_2 sample.

In summary, we report here a simple and scalable fast hydrolysis route to a three-dimensional flower-like iron doped rutile TiO_2 nanostructure. Characterization results reveal that iron species are evenly dispersed in the bulk rutile phase and on the surface. The replacement of tetravalent titanium atoms by trivalent iron atoms results in enhanced visible light absorption and promotes water dissociative adsorption. As a result, iron doped TiO_2 samples exhibit remarkable activity in visible-light-driven oxygen evolution from water splitting and an oxygen evolution rate of 154 μmol h^{-1} g_{cat}^{-1} can be achieved using the optimized 0.3% Fe–TiO_2 photocatalyst. This work might shed light on the rational design of doped semiconductors for target photocatalytic applications and improve our understandings on the roles of doping elements.

Acknowledgements

This work is supported by the National Natural Science Foundation of China (21421001), the Ministry of Education of China (IRT13022) and the 111 project (B12015).

Notes and references

1 A. Fujishima and K. Honda, *Nature*, 1972, **238**, 37.
2 M. R. Hoffmann, B. T. Martin, W. Choi and D. W. Bahnemann, *Chem. Rev.*, 1995, **95**, 69.
3 D. M. Schultz and T. P. Yoon, *Science*, 2014, **343**, 6174.
4 T. L. Thompson and J. T. Yates, *Chem. Rev.*, 2006, **106**, 4428.
5 Y. Ma, X. Wang, Y. Jia, X. Chen, H. Han and C. Li, *Chem. Rev.*, 2014, **114**, 9987.
6 J. Zhang, Q. Xu, Z. Feng, M. Li and C. Li, *Angew. Chem., Int. Ed.*, 2008, **47**, 1766.
7 T. M. Suzuki, G. Kitahara, T. Arai, Y. Matsuoka and T. Morikawa, *Chem. Commun.*, 2014, **50**, 7614.
8 C. Wang, D. W. Bahnemanna and J. K. Dohrmann, *Chem. Commun.*, 2000, 1539.
9 K. E. Karakitsou and X. E. Verykios, *J. Phys. Chem.*, 1993, **97**, 1184.
10 F. Zuo, L. Wang, T. Wu, Z. Zhang, D. Borchardt and P. Feng, *J. Am. Chem. Soc.*, 2010, **132**, 11856.
11 X. B. Chen, L. Liu, P. Y. Yu and S. S. Mao, *Science*, 2011, **331**, 746.
12 L. Li, J. Yan, T. Wang, Z.-J. Zhao, J. Zhang, J. Gong and N. Guan, *Nat. Commun.*, 2015, **6**, 5881.
13 K. Maeda, *Chem. Commun.*, 2013, **49**, 8404.
14 S. Chen, S. Shen, G. Liu, Y. Qi, F. Zhang and C. Li, *Angew. Chem., Int. Ed.*, 2015, **54**, 3047.
15 J. Tang, J. R. Durrant and D. R. Klug, *J. Am. Chem. Soc.*, 2008, **130**, 13885.
16 H. Sheng, H. Zhang, W. Song, H. Ji, W. Ma, C. Chen and J. Zhao, *Angew. Chem., Int. Ed.*, 2015, **54**, 5905.

17 M. Liu, X. Qiu, M. Miyauchi and K. Hashimoto, *J. Am. Chem. Soc.*, 2013, **135**, 10064.
18 J. Yan, G. Wu, N. Guan, L. Li, Z. Li and X. Cao, *Phys. Chem. Chem. Phys.*, 2013, **15**, 10978.
19 J. Yan, G. Wu, N. Guan and L. Li, *Appl. Catal., B*, 2014, **152–153**, 280.
20 H. Yu, H. Irie, Y. Shimodaira, Y. Hosogi, Y. Kuroda, M. Miyauchi and K. Hashimoto, *J. Phys. Chem. C*, 2010, **114**, 16481.
21 W. Feng, G. Wu, L. Li and N. Guan, *Green Chem.*, 2011, **13**, 3265.
22 O. Bikondoa, C. L. Pang, R. Ithnin, C. A. Muryn, H. Onishi and G. Thornton, *Nat. Mater.*, 2006, **5**, 189.
23 M. Ahmad, Y. Shi, A. Nisar, H. Sun, W. Shen, M. Wei and J. Zhu, *J. Mater. Chem.*, 2011, **21**, 7723.
24 M. Liu, L. Piao, W. Lu, S. Ju, L. Zhao, C. Zhou, H. Li and W. Wang, *Nanoscale*, 2010, **2**, 1115.
25 V. E. Henrich and A. F. Cox, *The Surface Science of Metal Oxides*, Cambridge University Press, 1993.
26 S. R. Morrison, *Electrochemistry at Semiconductor and Oxidized Metal Electrodes*, Plenum Press, 1980.
27 H. Tada, Q. Jin, H. Nishijima, H. Yamamoto, M. Fujishima, S. Okuoka, T. Hattori, Y. Sumida and H. Kobayashi, *Angew. Chem., Int. Ed.*, 2011, **123**, 3563.
28 C. C. Wang, K. W. Wang and T. P. Perng, *Appl. Phys. Lett.*, 2010, **96**, 143102.
29 K. Maeda, *ACS Catal.*, 2014, **4**, 1632.
30 S. Ikeda, N. Sugiyama, S. Murakami, H. Kominami, Y. Kera, H. Noguchi, K. Uosaki, T. Torimoto and B. Ohtani, *Phys. Chem. Chem. Phys.*, 2003, **5**, 778.

